Auxeticity from the Folded Geometry: a Numerical Study

Yu Chen, Adeel Zulifqar, Hong Hu*

Institute of Textile and Clothing, The Hong Kong Polytechnic University, Hung Hom, Kowloon, Hong Kong, PR China

* The corresponding author: hu.hong@polyu.edu.hk (Hong Hu); Tel.: +852-3400-3089

Abstract The folded geometry has successfully been transformed into auxetic woven fabric in the literature. However, the influences of the micro-geometric parameters on the macroscopic behavior have not been addressed yet. In this paper, several key micro-geometric parameters for the folded geometry were identified and the mechanical behaviors of the folded structure were preliminarily studied by using the finite element method. The results showed that the folded structure can be unfolded in both longitudinal and transverse directions when stretched and thus achieving a negative Poisson's ratio. More interestingly, another fantastic property of tension-bending coupling effect was found in the folded structure and a competition exists between the auxeticity and the tension-bending coupling effect. This is the first time to report a structure that can stimulatingly have the auxeticity and the tension-bending coupling effect. Due to the unique properties, the folded geometry is very promising in some important fields, examples being the textiles, civil engineering and auto industry. The present work may provide a good guide for the design and application of the folded structure.

Keywords Folded geometry, Finite element method (FEM), Negative Poison's ratio (NPR), Tension-bending coupling effect, Thin-walled structure

1. Induction

Negative value of Poisson's ratio does not contradict the classical elasticity [1], although it sounds incredible. A worldwide upsurge of research on those materials with negative Poisson's ratio (NPR) started from 1980s, after the pioneering work by Wojciechowski et al. [2, 3] and Lakes [4]. The terminology of "auxetics", that is commonly used today, was introduced by Evans et al. [5] in 1991 to name the NPR materials. It was found that the unique auxetic effect endows these materials with high shear modulus, indentation resistance, energy absorbance, vibration damping, sound absorption, and synclastic behavior for better formability, and thus finding a vast number of applications [6].

Over the past three decades, a considerable number of auxetic materials or structures have been developed, synthesized or fabricated from the macroscopic to the molecular levels, including foams, honeycombs, fabrics, composites, nanonetworks, graphene monolayers and so on [6-11]. In the meanwhile, the mechanisms for generating the auxetic effect have also been exploited in depth. It was found that the auxetic effect is gained predominantly from shape of microstructure rather than their chemical composition, and three mature mechanisms for NPR have been identified, which are re-entrant, rotation and elastic instability [12, 13]. The auxetic foam developed by Lakes [4] in 1987 was a typical re-entrant structure. Soon after Lakes' work, the re-entrant hexagonal honeycomb was theoretically reported to have NPR by Gibson and Ashby [14]. An amount of investigations have been conducted on the 2D re-entrant hexagonal configuration, examples being the mechanical modeling [14-18], the enhanced design [19-22] and the 3D extensions [23-26]. Other forms of re-entrant structures, such as, the star-shaped [27] and the double-ahead honeycombs [28, 29] were also well documented. Regarding rotation mechanism, there are two types of structures which can realize NPR by micro-structural rotation: chiral geometry [30-36] and rotating rigid-units structure [37-41]. The chiral unit comprises a central cylinder encapsulated in

tangentially attached ligaments, which is not superimposable on its mirror image. When the chiral structure is subjected to an external compression, the cylinder will rotate, causing the ligaments to flex and thus a NPR. The rotating rigid-units structure is engineered by several rigid units whose vertices are connected by hinges. The rigid units will rotate at the vertices under loading. The instability mechanism for NPR was firstly introduced by Bertoldi et al. [13] in the structure with ellipse holes. Unlike the re-entrant and the rotational structures, the auxetic effect in the holes structure is only found above a critical value of a compression strain. Since then, the instability mechanism for NPR has been implemented to many other structures [42-47].

All the auxetic examples above mentioned are the beam-like or void structures. How to obtain an auxetic continuum that does not contain voids is a curious issue and respectable attempts have been made in recent years. Salit and Weller [48] numerically investigated the mechanical behavior of a wrinkled membrane and proved the feasibility of introducing auxetic behavior into thin-walled structures. Grima et al. [49] demonstrated that the graphene could be made to mimic the behavior of the wrinkled paper model to exhibit auxetic properties. In particular, the folded geometry, as shown in Figure 1(a), has been successfully transformed to NPR fabrics (Figure 1(b)) by Cao et al. [50] and Zulifqar et al. [51]. This kind of fabrics could also be considered as a non-porous sheet or membrane and they were realized by creating the phenomenon of differential shrinkage into a fabric structure in order to enable different sections of a fabric unit cell to endure different levels of shrinkage upon relaxation. The relaxed fabric in Figure 1(b) can be divided into two sections, the loose weave zigzag area and the tight weave zigzag area. The former area deforms more easily than the later one under stretching. The previous work [50, 51] has performed details on the fabrication and mechanical behaviors of the fabrics and has revealed that auxetic behavior could be obtained under both warp and weft directional tensions. The work also suggested that these fabrics could be

applied for clothes that require enhanced shape fit and comfort.

However, the previous work lacked detailed discussion on the micro-geometry of the folded model, which is unfavorable for the modifications and applications of the folded geometry into fabric. Actually, it is quite difficult to precisely manipulate the micro-geometry of the folded structure into a fabric structure during the manufacturing process due to shrinkage control. While it is inconvenient to experimentally investigate the influence of the microscopic geometric parameters on the macroscopic behavior, the finite element (FE) method can be a powerful tool for these parameters studies. In the present work, several key micro-geometric parameters for the folded geometry were identified. The auxetic behavior of the folded structure and its dependence on the geometric and material parameters were preliminarily exploited by using the FE simulations. Finally, the deformation model of the folded structure was fully discussed.

2. Model and method

By parameterizing the folded fabric previously investigated by Cao et al. [50] and Zulifqar et al. [51], a folded model was built, as shown in Figure 2. The folded structure can be considered as a thin-walled structure without any voids. The thickness of the structure (see Figure 2(a)), T, is much smaller compared to the whole dimension. There are three key geometric parameters for determining the morphology in the *x*-*y* plane: l and θ for determining the zigzag strip in *x*-*y* plane while L elevating the distance between each two adjacent zigzag strips. In the view of the *z*-*y* plane, cross section of the zigzag strip is characterized by a single hump curve. From Figure 2(c), the single hump curve is built by using the "spline" feature in SOLIDWORKS based on the circle with a radius of R (R=1mm in the present work). It should be noted that, the role of the single hump fashion is only to make sure the whole structure has enough extension space when it undergoes an

external stress. For what, the single hump cure can be substituted by others fashions, for example an arch.

The folded geometry in this study was modeled using the SOLIDWORKS 3D CAD software. Firstly, the zigzag paths on the *x*-*y* plane were inserted. A new work plane which is perpendicular to each zigzag curve was built and a single hump sketch was drawn on each newly developed plane. Then, the zigzag folded strips were generated through the "swept" feature. One can also find from Figure 2(b) that the whole structure is formed by a periodically arrangement of a unit cell.

Once the model was generated, it would be finally imported into ANSYS/Workbench for analysis and the material and its properties would be assigned to it. The basic material for the folded structure is determined according to the specific application. For most energy absorption purposes, metal is widely chosen while the relatively soft materials are generally used in the textile industry for comfort purpose. Here, the moduli of the basic material (see Table.1) were chosen by reference of the experimental results of a basic woven fabric we produced, which is generally recognized as an orthotropic body. A compliance matrix, as shown in Equation (1), is used to define the orthotropic behavior of the fabric:

$$\begin{pmatrix} \hat{\varepsilon}_x \\ \hat{\varepsilon}_y \\ \hat{\varepsilon}_z \\ \hat{\gamma}_{xy} \\ \hat{\gamma}_{yz} \\ \hat{\gamma}_{xz} \end{pmatrix} = \begin{bmatrix} \frac{1}{\hat{E}_x} & \frac{-\hat{\nu}_{xy}}{\hat{E}_y} & \frac{-\hat{\nu}_{xz}}{\hat{E}_z} & 0 & 0 & 0 \\ \frac{-\hat{\nu}_{yx}}{\hat{E}_x} & \frac{1}{\hat{E}_y} & \frac{-\hat{\nu}_{yz}}{\hat{E}_z} & 0 & 0 & 0 \\ \frac{-\hat{\nu}_{zx}}{\hat{E}_x} & \frac{-\hat{\nu}_{zy}}{\hat{E}_y} & \frac{1}{\hat{E}_z} & 0 & 0 & 0 \\ 0 & 0 & 0 & \frac{1}{\hat{G}_{xy}} & 0 & 0 \\ 0 & 0 & 0 & 0 & \frac{1}{\hat{G}_{yz}} & 0 \\ 0 & 0 & 0 & 0 & 0 & \frac{1}{\hat{G}_{xz}} \end{bmatrix} \begin{pmatrix} \hat{\sigma}_x \\ \hat{\sigma}_y \\ \hat{\sigma}_z \\ \hat{\sigma}_{xy} \\ \hat{\sigma}_{yz} \\ \hat{\sigma}_{xz} \end{pmatrix}. \quad (1)$$

In Equation (1), the symbols *x* and *y* respectively denotes the weft and warp direction in Figure 1

while z is the direction perpendicular to the x-y plane. There are only 9 independent constants in Equation (1) according to the reciprocal relations:

$$\hat{E}_x\hat{\nu}_{yx} = \hat{E}_y\hat{\nu}_{xy},\ \hat{E}_y\hat{\nu}_{zy} = \hat{E}_z\hat{\nu}_{yz},\ \hat{E}_z\hat{\nu}_{xz} = \hat{E}_x\hat{\nu}_{zx}. \quad (2)$$

The explicit dynamics has been proven to be valuable in quasi-static problems [52-55], and thus the Explicit Dynamics (LS-DYNA Export) module in ANSYS/Workbench was used for simulations here. Figure 3 illustrates the detailed boundary conditions we used. When stretching along the x direction (Figure 3(a)), the left boundary of the model was fixed along the x direction and a uniform x-directional displacement was applied on the right boundary. In order to simulate a real tensile test environment, the y- and z- directional displacements of both the left and right boundaries were constrained. For y- directional stretching (Figure 3(b)), the x- and z- directional displacements on both the top and bottom boundaries were zero. The bottom of the model was fixed along the y direction while stretching the top boundary.

Under longitudinally tension, a series of quasi-uniform wavy shape can be observed in the transverse sides, as shown in Figure 4. The calculation procedure for the Poisson's ratio of the folded structure was introduced as follows:

By using the post processor, LS-PrePost, we can readily record the displacement of the every node in the structure. In the case of x- directional tension, the left and right boundaries are kept in flat during deformation (see Figure 4(a)). L and R is the point on the left and boundary, respectively. Therefore, it is easy to obtain the longitudinal strain (ε_x) as:

$$\varepsilon_x = \frac{x_{\mathrm{R}}^{\tau} - x_{\mathrm{L}}^{\tau}}{x_{\mathrm{R}}^{0} - x_{\mathrm{L}}^{0}} - 1, \quad (3)$$

where x_L^{τ} and x_R^{τ} respectively denotes the x- directional coordinate of the points L and R at time τ, while x_L^0 and x_R^0 denotes the x- directional coordinate at time 0. The point T is the peak of the

top boundary while point B is trough of the bottom boundary. The transverse strain (ε_y) can be given as:

$$\varepsilon_y = \frac{y_{\mathrm{T}}^{\tau} - y_{\mathrm{B}}^{\tau}}{y_{\mathrm{T}}^{0} - y_{\mathrm{B}}^{0}} - 1, \tag{4}$$

with y_{T}^{τ} and y_{B}^{τ} respectively denotes the *y*- directional coordinate of the points T and B at time τ, while y_{T}^{0} and y_{B}^{0} denotes the *y*- directional coordinate at time 0. Finally, the Poisson's ratio is calculated as:

$$\nu_{xy} = -\frac{\varepsilon_y}{\varepsilon_x}. \tag{5}$$

The Poisson's ratio (ν_{yx}) when stretching along the *y* direction (Figure 4(b)) can be obtained via the similar procedure. What should be underscored is that the transverse true strain is calculated by the coordinate of the selected points (points T and B in Figure 4(a) and points L and R in Figure 4(b)), and thereby the position of the selected points may lead to an fluctuation in the result. For accuracy, these points should be as close as possible to the midpoint of the transverse sides.

The efficiency and accuracy are the two main key factors for the simulations. They deeply depend on both the meshes and loading rate and should be taken into considerations seriously during simulations. As we know, the smaller mesh size and the lower loading rate, the higher accuracy will be, but the larger computation time will simultaneously be needed. Therefore, a trade off should be made between the efficiency and accuracy, and two questions are raised: (a) how big should the mesh size be? (b) how large should the loading rate be?

For a good quality of meshes, the "tetrahedrons" scheme was set for all the folded models. A proper mesh size for each case can be determined by comparing the results calculated from various meshes. We implemented three mesh sizes of 0.3mm, 0.25mm and 0.2mm to the folded structure with L=4mm，l=4mm, θ=45° and three levels of T, i.e., T=0.15mm, T=0.10mm and T=0.05mm.

The relations between the transverse true strain, ε_y, and the longitudinal true strain, ε_x, of the structure are illustrated in Figure 5(a), (c) and (e). It was found that, for the structures with three different levels of T, the results obtained from 0.3mm mesh size are close to those obtained from 0.25mm and 0.2mm sizes. Consequently, the mesh size of 0.3mm is suitable for these cases. By using the similar mesh sensitivity analysis, 0.3mm mesh size was determined for all of the FE cases in this paper.

In the present work, a low loading rate of 0.025m/s was adopted. As summarized by Nasim and Etemadi [55], there are two simple criteria that can be used to confirm the accuracy:

(a) The kinetic energy should be much lower than the internal energy [56];

(b) The diagram of forces does not significantly change under different velocities [52, 56, 57].

The first of the criteria was adopted to verify whether the set loading rate (0.025m/s) is suitable for quasi-static analysis. Figure 5 (b), (d) and (f) illustrate the internal and kinetic energies histories of the folded structures (L=4mm，l=4mm, θ=45° and three different levels of T: 0.15mm, 0.1mm, 0.05mm) when stretching at a speed of 0.025m/s along the x direction. It was clearly shown that the kinetic energy is very low and close to zero. This criterion was implemented to all of other cases and similar results were obtained.

3. Results and discussion

3.1. Parameters studies

This section aims to exploit the influences of the key parameters (L, l, θ and T) on the auxetic behavior of the folded structure. Here, a block with 9×9 unit cells was adopted for all of the FE models.

From the view of the x-y plane (Figure 1(b)), the zigzag strips will gradually unfold under

longitudinal tension, which leads to an expansion in the transverse direction. Figure 6 displays the variations of the Poisson's ratio with the longitudinal strain under three different levels of L. An obvious auxecity can be observed in the folded structures under both *x*- and *y*- directional tension and the smaller L is, the more obvious the auxeticity. This is because the smaller L is, the lower effect from the region between each two adjacent zigzag strips (called thin-plated region). Structurally, the zigzag strips will expand in transverse direction under longitudinal tension but the thin-plated region will shrink transversely. Therefore, the thin-plated region will diminish the auxeticity of the structure. It is also remarkable that the auxeticity sharply increases at small strain and then gradually decreases with strain increasing. Similar variations of the Poisson's ratio with the strain are observed in Figure 7, which also reveals the effects of the slant angle, θ, on the Poisson's ratio. In both *x*- and *y*- directional tension, as shown respectively in Figure 7 (a) and (b), the larger the slant angle is, the more obvious the auxeticity. This is because the structure has more space to expand transversely with larger slant angle.

The effects of the parameter *l* on the Poisson's ratio were illustrated in Figure 8. At the small level of applied strain, the value of *l* does not influence the Poisson's ratio much. With the strain increasing, the influence of *l* progressively becomes significant: the larger *l* is, the more obvious the auxeticity when stretching along the *x* direction, but an opposite result is obtained under *y*-directional tension. As a result, *l* can thereby be manipulated to balance the auxetic performance between two principal directions.

The folded geometry is a successful example of introducing the auxeticity into the thin-walled structure. Another focus in this paper is how the thickness (T) affects the behavior. The folded structure with three levels of thickness, 0.05mm, 0.10mm and 0.15mm, were investigated here. A shown in Figure 9, the structure with 0.10mm thickness shows almost similar Poisson's

ratio with 0.15mm thickness structure, under both *x*- and *y*- directional tension. It is remarkable that the structure with lowest T shows the largest auxeticity at small strain but almost the similar Poisson's ratio value to that of the 0.10mm and 0.15mm thickness structures at large strain. Two conclusions can thereby be drawn from the above analysis: (a) under small strain, the thinner the thickness is, the more obvious the auxeticity. This is because the folded structure with thinner thickness easier expands under tension at low strain. However, the Poisson's ratio of the structure with thinner thickness will finally be close to that of the structure with thicker thickness at large strain as the folded structure becomes unfolded; (b) for thicker thickness structures, their Poisson's ratio is nearly independent of the thickness. These conclusions are very valuable to the design and application of this kind of thin-walled structure.

3.2. Tension-bending coupling effect

This section compares the Poisson's ratio from the folded structures with four different levels of cell numbers (N×N): 9×9, 11×11, 15×15 and 20×20 cells. Intuitively, the boundary effect will decreases with the increase of the cell number and then the more the cell number is, the larger the NPR value. However, a completely opposite result shown in Figure 10 is that the auxeticity diminishes with the cell number increasing. Such an abnormal phenomenon is caused by another unique property of the folded structure, called tension-bending coupling effect. The tension-bending coupling effect is illustrated in Figure 11, in which an out of plane bending behavior occurs when the folded structure is stretched along the *x*- or *y*- direction (in-plane). As mentioned before, when the folded structure undergoes a uniaxial tension, the folded zigzag strips will get unfolded, leading to a transverse expansion. On the contrary, the thin-plated region between each two adjacent strips tends to contract. This opposite trend in deformation will result in an inconformity in displacement

or stress and thus forming the tension-bending coupling effect.

Obviously, a competition exists between the auxeticity and the tension-bending coupling effect as the tension-bending coupling effect will reduce the transverse expansion under longitudinal tension. Figure 11 illustrates the deformation modes of the folded structure with different cell numbers. Obvious bending phenomenon can be observed. It is also found that an earlier bending phenomenon starts in the folded structure with larger cell number. Under the same strain, the larger the cell number is, the more obvious the tension-bending coupling effect.

4. Conclusions

The folded geometry forms the basis of this paper. Several key micro-parameters including L, l, θ and T were identified and their influences on the macroscopic behavior of the structure were systematically analyzed by using the FEM. The tension-bending coupling effect of the structure was also discussed based on the FE models with different cell numbers. The study first confirms that a folded thin-walled structure can simultaneously have the auxeticity and the tension-bending coupling effect and this finding is very encouraging. These unique properties are only related to the micro-geometry but independent of the basic materials used. The folded geometry is very promising in many important fields. The folded structure developed by woven fabric of other soft materials is suitable for clothing applications as it can fully satisfy the enhanced shape fit and comfort requirements. Apart from that, the folded geometry can be used as a flexible membrane structure in the architectural and civil engineering and it can also be made into a thin-walled energy absorber in auto industry. For fully understanding the structure, more issues will be addressed next, including the experimental evaluation, energy absorption.

Acknowledgement

The authors would like to thank the funding support from the Research Grants Council of Hong Kong Special Administrative Region Government (grant number: 15205514) and The Hong Kong Polytechnic University (internal project reference: YBUZ).

Conflict of interest statement

The authors declare that they have no conflict of interest.

References

[1] K.W. Wojciechowski, *J. Phys. Soc. Jpn.* **2003**,72(7),1819.
[2] K. W. Wojciechowski, *Mol. Phys.* **1987**,61(5),1247.
[3] K.W. Wojciechowski, A. C. Branka, *Phys. Rev. A* **1989**,40(12),7222.
[4] R. Lakes, *Science* **1987**, 238, 551.

[5] K. E. Evans, M. A. Nkansah, I. J. Hutchinson, S. C. Rogers, *Nature* **1991**, 353(6340), 124.

[6] H. Hu, M. Zhang, Y. Liu, Woodhead Publishing, **2019**.

[7] T. C. Lim, Springer, Singapore, **2015**.

[8] S. Naik, R. D. Dandagwhal, C. N. Wani, S. K. Giri, AIP Conference Proceedings **2019**, 2105(1): 020004.

[9] J. N. Grima-Cornish, J. N. Grima, K. E. Evans, *phys. Status Solidi B* **2017**,1700190.

[10] J. N. Grima, M. C. Grech, J. N. Grima-Cornish, R. Gatt, D. Attard, *Ann. Phys. (Berlin)* **2018**, 530, 1700330.

[11] C. W. Smith, J. N. Grima, K. E. Evans, Acta Mater. **2000**, 48(17), 4349.

[12] H. M. A. Kolken, A. A. Zadpoor, *RSC Adv.* **2017**, 7, 5111.

[13] K. Bertoldi, P. M. Reis, S. Willshaw, T. Mullin, *Adv. Mater.* **2010**, 22(3),361.

[14] L.J. Gibson, M. F. Ashby, London: Pergamon Press **1988**.

[15] I. G. Masters, K. E. Evans, *Compos. Struct.* **1996**, 35(4),403.

[16] J. N. Grima, D. Attard, B. Ellul, R. Gatt, *Cell. Polym.* **2011**, 30(6),287.

[17] F. Scarpa, P. Panayiotou, G. Tomlinson, *J. Strain Anal. Eng. Des.* **2000**,35(5),383.

[18] H. Wan, H. Ohtaki, S. Kotosaka, G. Hu, *Eur. J. MECH. A-SOLID* **2004**, 23(1),95.

[19] Z. X. Lu, X. Li, Z. Y. Yang, F. Xie, *Compos. Struct.* **2016**,138, 243.

[20] M. H. Fu, Y. Chen, L. L. Hu, *Compos. Struct.* **2017**,160,574.

[21] M. H. Fu, Y. Chen, L. L. Hu,*Compos. Struct.* **2017**, 175, 101.

[22] Y. Chen, M. H. Fu, *Appl. Compos. Mater.* **2018**, 25,1041.

[23] L. Yang, D. Cormier, H. West, O. Harrysson, K. Knowlson, *Mater. Sci. Eng. A* **2012**,558,579.

[24] L. Yang, O. Harrysson, H. West, D. Cormier, *J. Mater. Sci*.**2013**,48(4),1413.

[25] L. Yang, O. Harrysson, D. Cormier, H. West, H. Gong, B. Stucker, *Jom. J. Miner. Met. Mater. Soc.* **2015**,67(3),608.

[26] L. Yang, O. Harrysson, H. West, D. Cormier, *Int. J. Solids. Struct.* **2015**,69-70,475.

[27] J. Meng, Z. Deng, K. Zhang, X. Xu, F. Wen, *Smart Mater. Struct.* **2015**, 24(9),095011.

[28] J. Qiao, C. Q. Chen, *J. Appl. Mech.* **2015,** 82(5),051007.

[29] J. X. Qiao, C. Q. Chen, *Int. J. Impact Eng.* **2015**, 83,47.

[30] D. Prall, R. S. Lakes, *Int. J. Mech. Sci.* **1997**, 39(3),305.

[31] A. Alderson, K. L. Alderson, D. Attard, K. E. Evans, R. Gatt, J. N. Grima, W. Miller, N. Ravirala, C. W. Smith, K. Zied, *Compos. Sci. Technol.* **2010**, 70(7),1042.

[32] A. Alderson, K. L. Alderson, G. Chirima, N. Ravirala, K. M. Zied, *Compos. Sci. Technol.* **2010**, 70(7),1034.

[33] A. Lorato, P. Innocenti, F. Scarpa, A. Alderson, K. L. Alderson, K. M. Zied, N. Ravirala, W. Miller, C. W. Smith, K. E. Evans, *Compos. Sci. Technol.* **2010**, 70(7),1057.

[34] C. S. Ha, M. E. Plesha, R. S. Lakes, *phys. Status Solidi B* **2016**, 253(7),1243.

[35] C. S. Ha, M. E. Plesha, R. S. Lakes, *Smart Mater. Struct.* **2016**, 25(5),054005.

[36] M. H. Fu, B. B. Zheng, W. H. Li, *Compos. Struct.* **2017**, 176,442.

[37] J. N. Grima, V. Zammit, R. Gatt, A. Alderson, K. E. Evans, *phys. Status Solidi B* **2007**, 244(3),866.

[38] J. N. Grima, K. E. Evans, *J. Mater. Sci. Lett.* **2000**, 19(17),1563.

[39] D. Attard, J. N. Grima, *phys. Status Solidi B* **2008**, 245(11),2395.

[40] J. N. Grima, R. Caruanagauci1, M. R. Dudek, K. W Wojciechowski, R. Gatt, *Smart Mater. Struct.* **2013**, 22,084016.

[41] D. Attard, E. Manicaro, J. N. Grima, *Phys. Status Solidi B* **2009**, 246(9),2033.

[42] A. Ghaedizadeh, J. Shen, X. Ren, Y. M. Xie, *Mater.* **2016**, 9(54),1.

[43] D. Mousanezhad, S. Babaee, H. Ebrahimi, R. Ghosh, A. S. Hamouda, K. Bertoldi, A. Vaziri, *Sci. Rep.* **2015**, 5,18306.

[44] K. Bertoldi, P. M. Reis, S. Willshaw, T. Mullin, *Adv. Mater.* **2010**, 22(3),361.

[45] S. Babaee, J. Shim, J. C. Weaver, E. R. Chen, N. Patel, K. Bertoldi, *Adv. Mater.* **2013**, 25(36),5044.

[46] J. Shen, S. Zhou, X. Huang, Y. M. Xie, *Phys. Status Solidi B* **2014**, 251(8),1515.

[47] X. Ren, J. Shen, A. Ghaedizadeh, H. Tian, Y. M. Xie, *Smart Mater. Struct.* **2015**, 24(95016).

[48] V. Salit, T. Weller, *Acta Mater.* **2009**, 57, 125.

[49] J. N. Grima, S. Winczewski, L. Mizzi, M. C. Grech, R. Cauchi, R. Gatt, D. Attard, K. W. Wojciechowski, J. Rybicki, *Adv. Mate.*. **2015**, 27, 1455.

[50] H. Cao, A. Zulifqar, T. Hua, H. Hu, *Text. Res. J.* 2019, 89(13), 2694.

[51] A. Zulifqar, T. Hua, H. Hu, *Text. Res. J.* **2018**, 88(18), 2076.

[52] L. Aktay, A. K. Toksoy, M. Guden, *Mater. Des.* **2006**,27,556.

[53] X. M. Xiang, G. Lu, Z. H. Wang, *Int. J. Mech. Sci.* **2015**,103,55.

[54] R. K. Fathers, J. M. Gattas, Z. You, *Int. J. Mech. Sci.* **2015**, 101-102,421.

[55] M. S. Nasim, E. Etemadi, *Int. J. Mech. Sci.* **2018**, 136,475.

[56] S. A. Meguid, J. C. Stranart, J. Heyerman, Finite Elem. Anal. Des. **2004**, 40(9-10),1035.

[57] S. P. Santosa, T. Wierzbicki, A. G. Hanssen, M. Langseth, *Int. J. Impact Eng.* **2000**, 24(5),509.

Table 1. Main parameters of the basic material.

$\hat{E}_x$ (MPa)	$\hat{E}_y$ (MPa)	$\hat{E}_z$ (MPa)	ν_{xy}	ν_{yz}	ν_{xz}	$\hat{G}_{xy}$ (MPa)	$\hat{G}_{yz}$ (MPa)	$\hat{G}_{xz}$ (MPa)
1.87	3.69	0.8	0.2	0.3	0.25	0.64	0.5	0.4

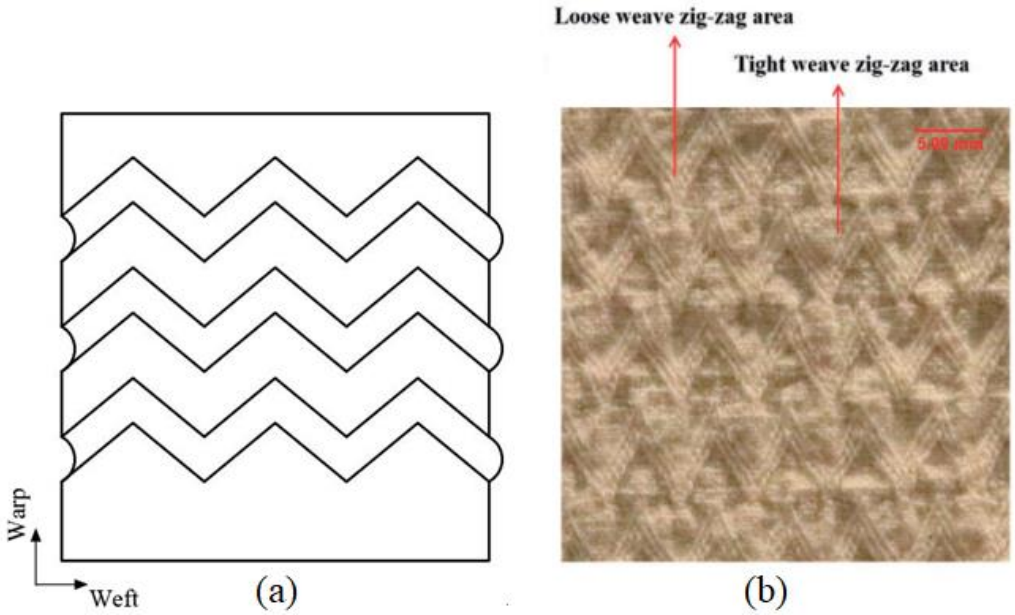

Figure1. (a) Schematic diagram of the folded geometry and (b) fabric face after relaxation [50]. (Color online only)

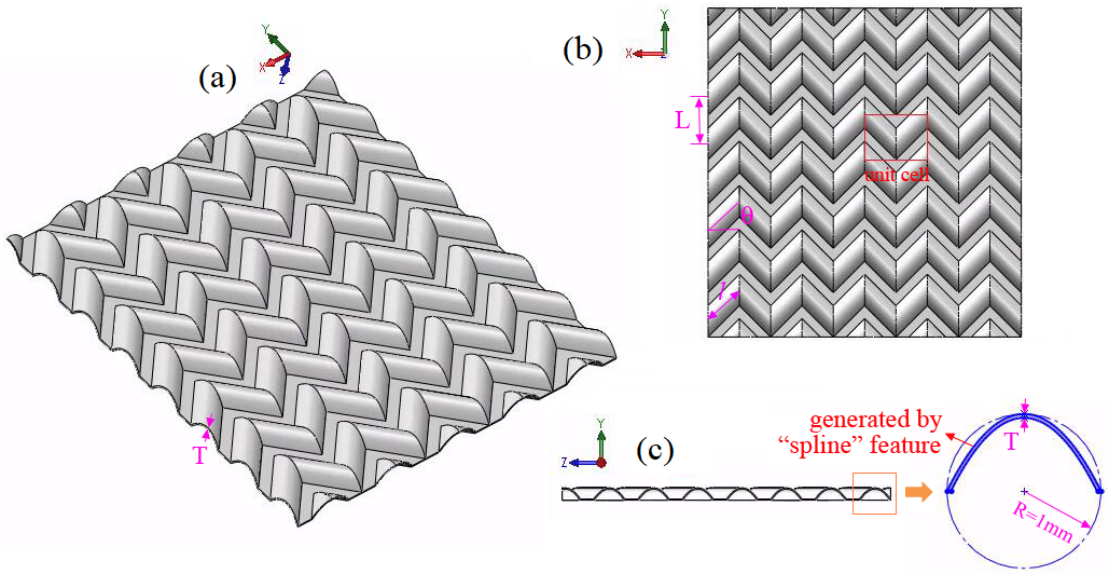

Figure 2. Parameterized folded geometry. (Color online only)

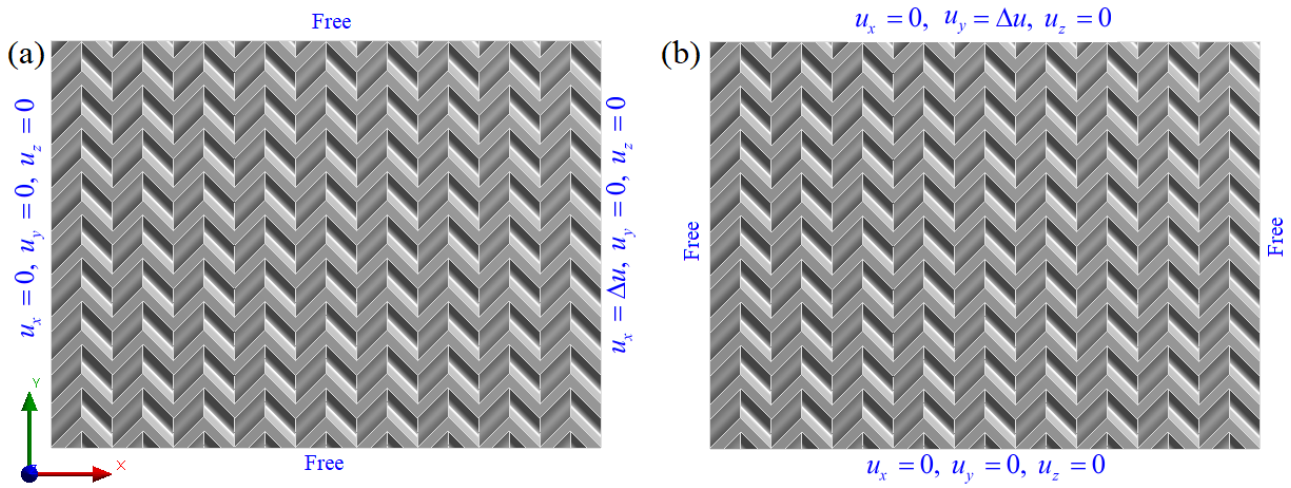

Figure 3. Boundary conditions used in FE simulations: (a) stretching along *x*- direction and (b) stretching along *y*- direction. (Color online only)

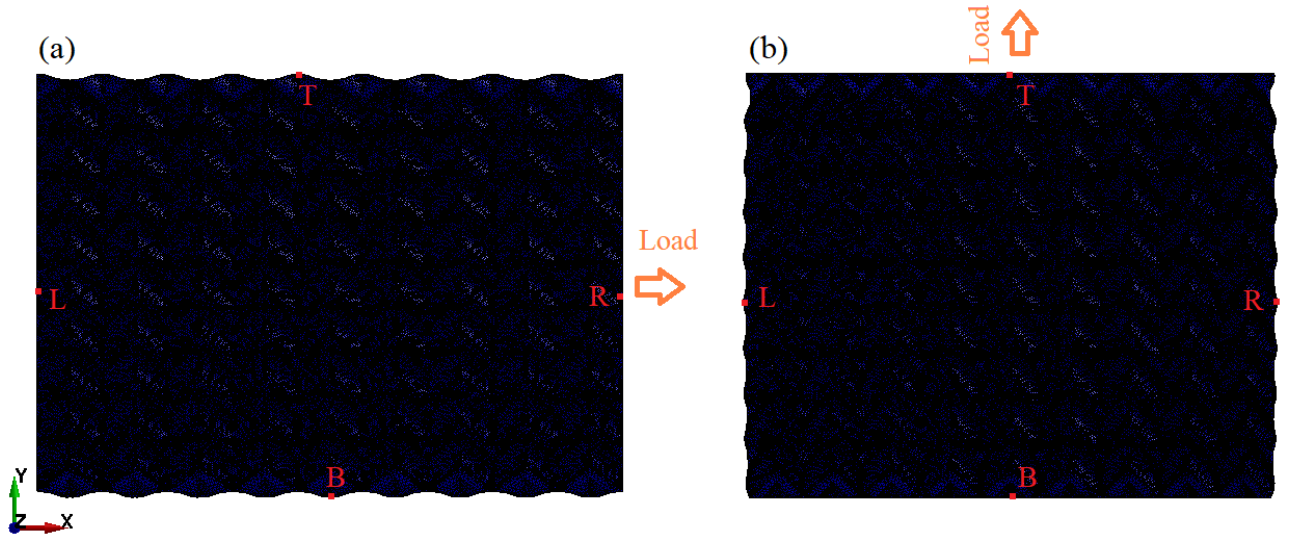

Figure 4. Schematic diagram of the deformation model of the folded structure: (a) stretching along the *x* direction and (b) stretching along the *y* direction. (Color online only)

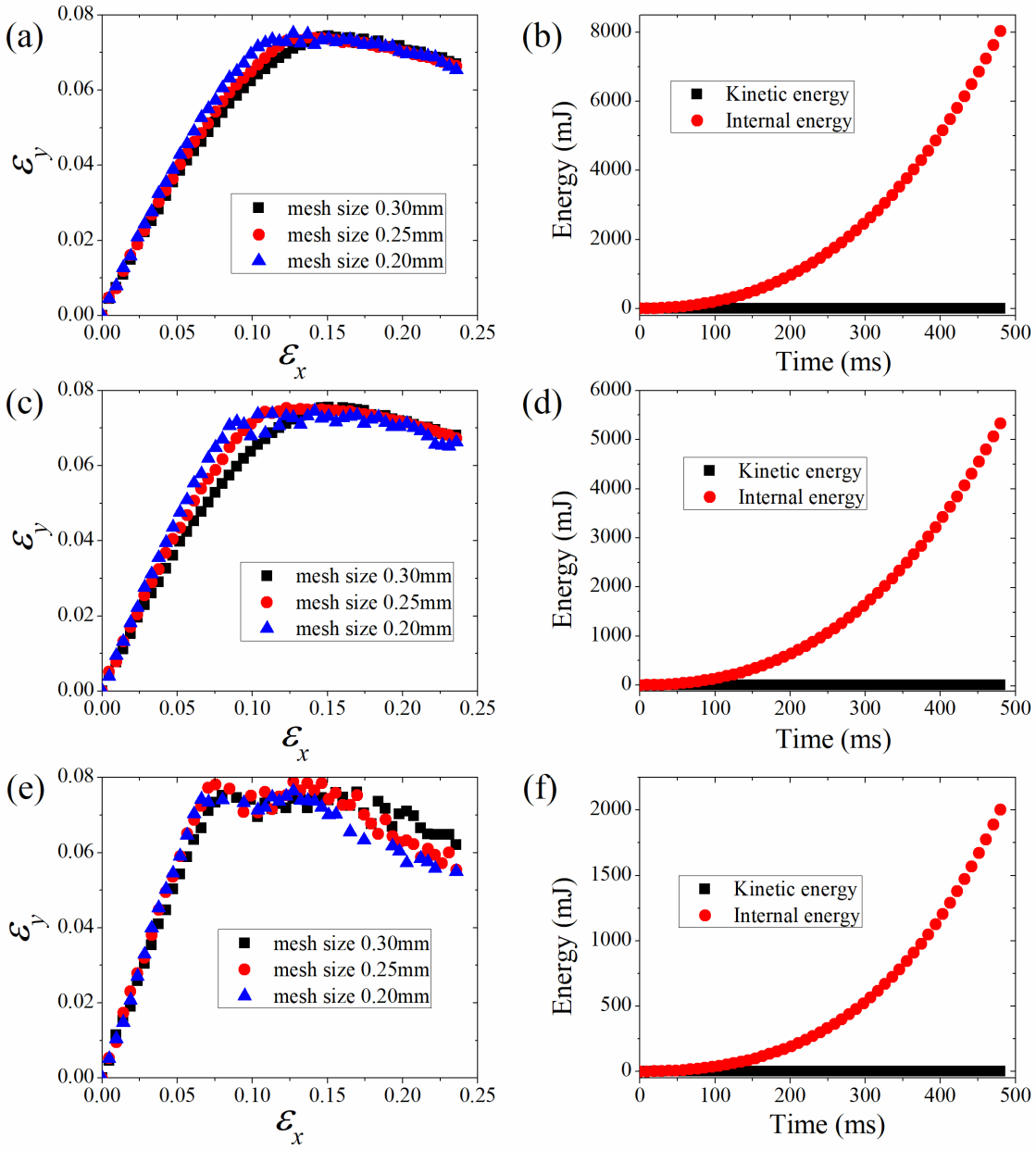

Figure 5. Variations of the transverse strain (ε_y) with longitudinal strain (ε_x) obtained from different mesh sizes and energy history diagrams respect to recognize quasi-static loading (L=4mm，l=4mm，θ=45°): (a) T=0.15mm; (b) T=0.15mm, 0.3mm mesh size; (c) T=0.10mm; (d) T=0.10mm, 0.3mm mesh size; (e) T=0.05mm; (f) T=0.05mm, 0.3mm mesh size. (Color online only)

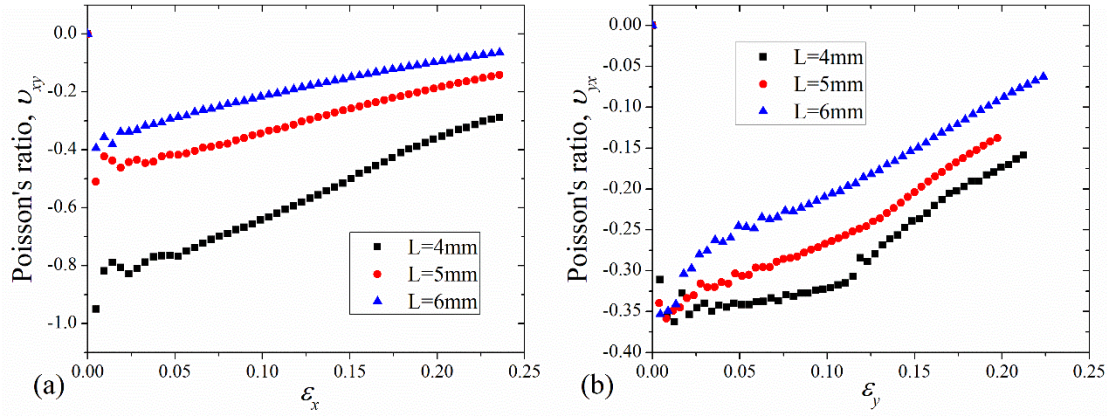

Figure 6. Effect of L on the Poisson's ratio of the folded structure (T=0.1mm, θ=45° , l=4mm): (a) stretching along the x direction, (b) stretching along the y direction. (Color online only)

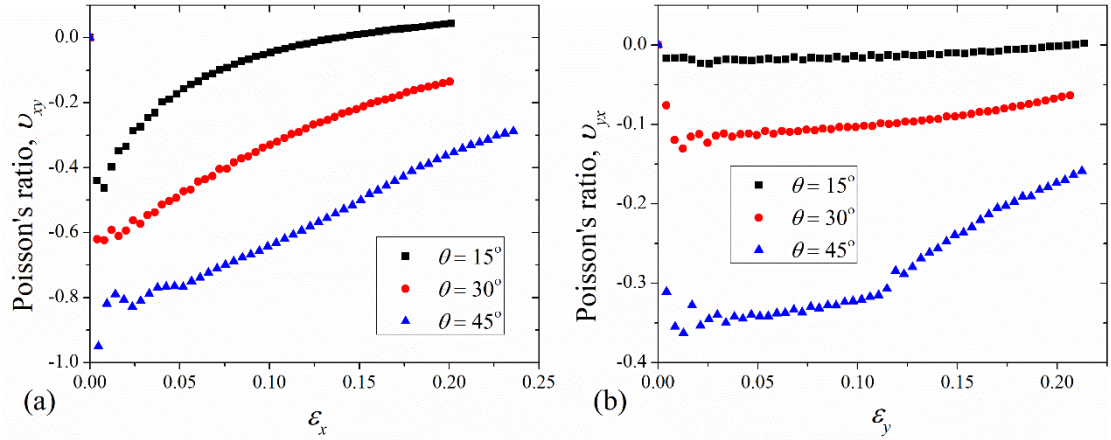

Figure 7. Effect of the slant angle, θ, on the Poisson's ratio of the folded structure (T=0.1mm, L=4mm, l=4mm): (a) stretching along the x direction, (b) stretching along the y direction. (Color online only)

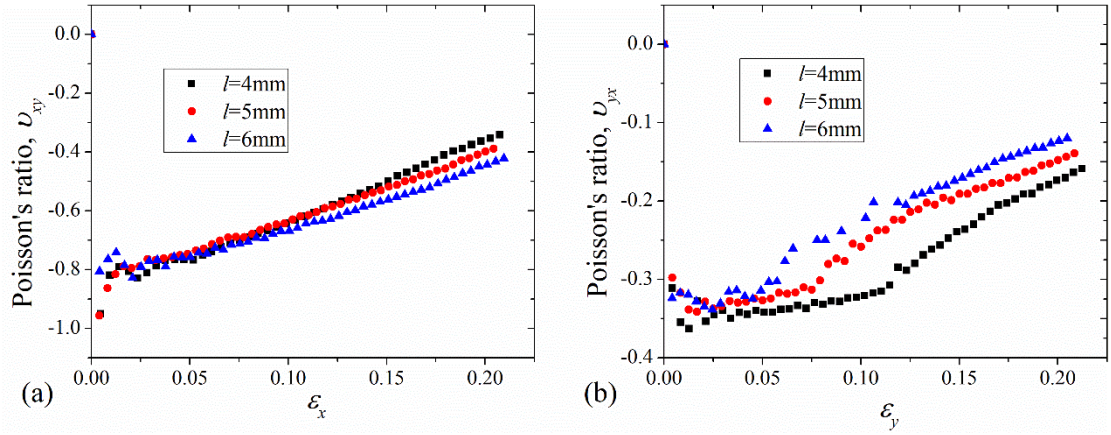

Figure 8. Effect of l on the Poisson's ratio of the folded structure (L=4mm, T=0.1mm , θ=45°): (a) stretching along the x direction, (b) stretching along the y direction. (Color online only)

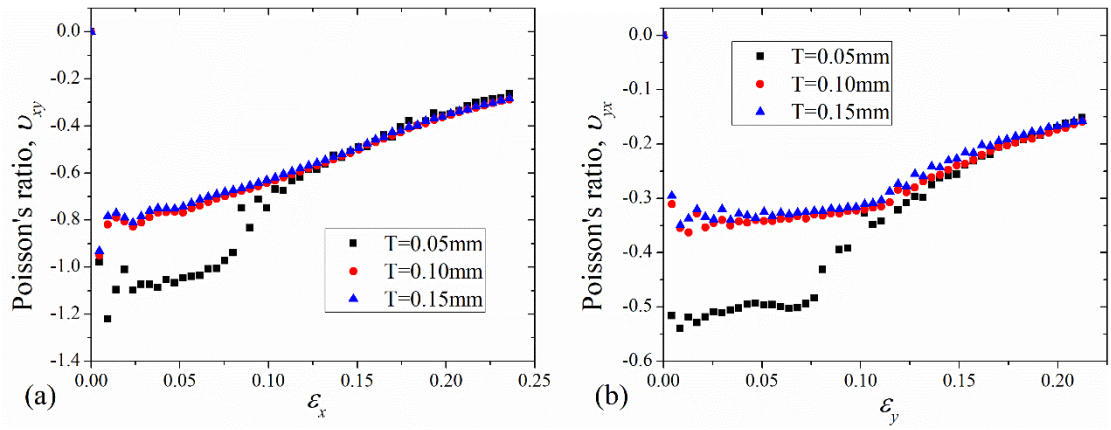

Figure 9. Effect of structure thickness, T, on the Poisson's ratio of the folded structure (L=4mm, *l*=4mm, θ=45°): (a) stretching along the *x* direction, (b) stretching along the *y* direction. (Color online only)

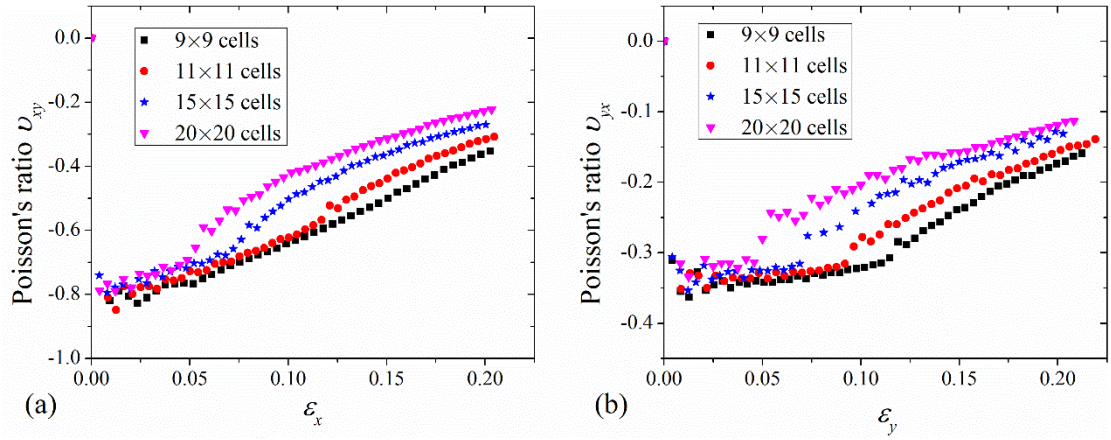

Figure 10. Effect of the cell numbers on the Poisson's ratio of the folded structure (L=4mm, *l*=4mm, T=0.1mm, θ=45°): (a) stretching along the *x* direction, (b) stretching along the *y* direction. (Color online only)

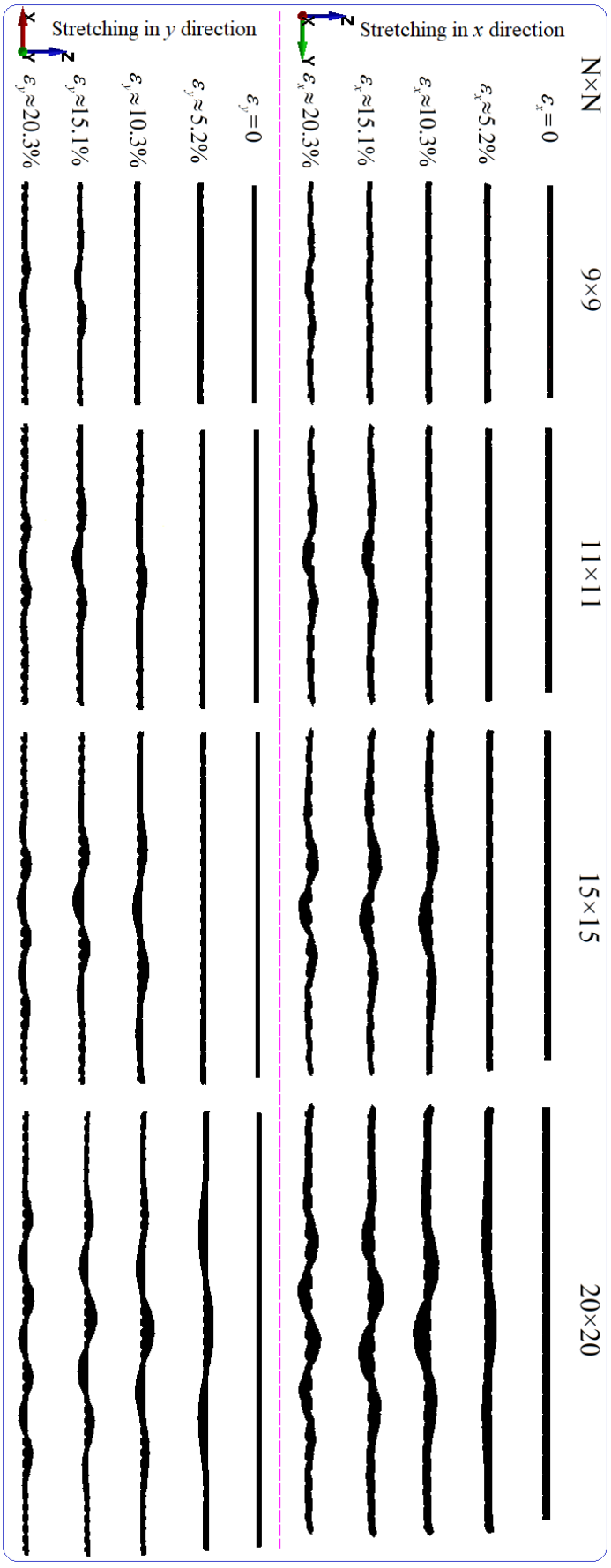

Figure 11. Deformation modes of the folded structure with different cell numbers. (Color online only)